ACS OMEGA

http://pubs.acs.org/journal/acsodf

Mini-Review

Patterning Liquid-Crystal Alignment for Ultrathin Flat Optics

Kun Yin, Jianghao Xiong, Ziqian He, and Shin-Tson Wu*

Cite This: *ACS Omega* 2020, 5, 31485−31489

Read Online

ACCESS | Metrics & More | Article Recommendations

ABSTRACT: Liquid-crystal (LC)-based ultrathin flat optical elements (FOEs) exhibit several attractive properties, such as a high degree of optical tunability, strong polarization selectivity, nearly 100% diffraction efficiency, and a simple fabrication process. Investigating the alignment patterning of LC-FOEs to diversify their performance has attracted broad interest in the optics field. In this mini-review, we start from the photoalignment (PA) process and then dive into device structures and performances. By generating and recording the desired polarization fields on the PA layer, the LC molecules will follow the recorded patterns and establish the phase profiles for different functionalities, such as gratings and lenses. Because of the polarization dependency, LC-FOEs have found useful applications in near-eye displays. Understanding the interactions between the PA mechanism and LC molecules helps to optimize the device performance for novel optical systems.

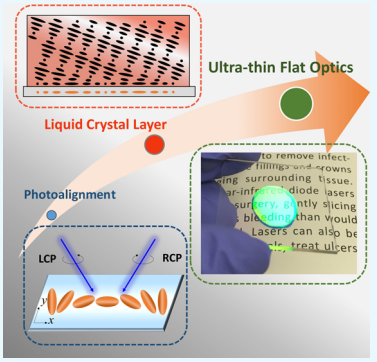

1. INTRODUCTION

Different from conventional refractive optics that use the optical path difference to produce phase patterns, liquid-crystal-based flat optical elements (LC-FOEs) generate the desired phase profile by spatially varying the LC orientations, which is controlled through the alignment patterning on the bottom surface.[1,2] Due to the distinct optical properties, such as a flat surface, ultrathin form factor, high diffraction efficiency, strong polarization dependency, and high optical quality, LC-FOEs have been successfully integrated into various optical systems to satisfy the increasing demands from near-eye displays[3,4] and head-up displays.[5]

The working principle of these planar optics is based on the modulation of the LC material's refractive index, which is established and controlled by the alignment patterning and the self-organization of LC molecules.[2] Among various approaches to obtain the desired surface alignment, including mechanical rubbing[6] and nanoimprinting lithography (NIL),[7] photoalignment (PA) has the advantages of high resolution, a simple and quick fabrication process, and low cost.[8] Compared to the novel method such as NIL, PA has been studied for decades. The origin can be traced back to the 1970s.[9] Then in 1988,[10] the first publication about LC PA appeared, which proposed the photoinduced alignment of a reversible transformation of azobenzene molecular layers. The LC alignment was induced by controlling the wavelength of an unpolarized light beam. Subsequently, Gibbons et al. reported the surface-mediated alignment of nematic LCs with a polarized light in 1991.[11] The LC alignment is induced by exposing a dye-doped polymer layer to the polarized light. The LC molecules in contact with the illuminated area were homogeneously aligned perpendicular to the laser polarization direction and remained aligned after the laser beam was turned off. Since 1992, the cinnamoyl side-chain polymers and polyimide aligning agents have been used for LC alignment.[12] Nowadays, the class of azo dyes is widely used for recording alignment patterns of LC-based optics. Through controlling the alignment, LC-FOEs can exhibit various functional properties,[13,14] which is not only scientifically interesting but also practically useful.

2. LIQUID-CRYSTAL PHOTOALIGNMENT

2.1. Mechanism of Photoalignment. The LC molecular orientation results from photoinduced absorption in an amorphous film (PA layer) formed by anisotropic absorbing molecular units (PA materials).[8] This process can generally be divided into two types: reversible transformation[15,16] and irreversible transformation.[12,17] For each type, it can also be further classified based on different chemical reactions and molecular motions. Compared to the irreversible photochemical changes, the reversible type involving azo dyes shows a higher purity of alignment layer, which is favorable for numerous LC-based applications including flat optics.

The PA mechanism in the proposed LC-FOEs belongs to the reversible type, and this process can be described by the diffusion model of azo dye chromophore molecules or azo dye molecular solutes. As Figure 1a depicts, the azo dye molecules are exposed under a polarized UV light. The angle between the

Received: October 18, 2020
Accepted: November 20, 2020
Published: December 3, 2020

https://dx.doi.org/10.1021/acsomega.0c05087
ACS Omega 2020, 5, 31485−31489

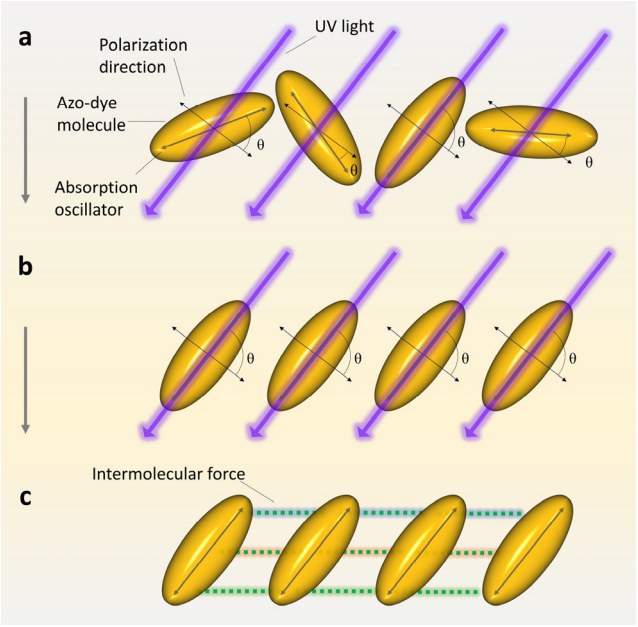

Figure 1. Mechanism of the PA process. (a) Azo dyes are exposed to a linearly polarized UV light, (b) reorientation occurs, and (c) mechanism is locked by the intermolecular forces.

absorption oscillator of the molecule and the polarization direction is defined as θ. For each azo dye molecule, the probability to absorb light energy is proportional to $\cos^2\theta$.[8] When the molecule is parallel to the polarization direction, the probability is the highest; that is, it is most likely to obtain increased internal energy through absorption. This increased energy leads to a more active rotational motion until the absorption oscillator is perpendicular to the polarization direction, as shown in Figure 1b. Therefore, all or most of the azo dye molecules are tempting to rotate and align the long axes perpendicular to the polarization direction of the UV light. After orientation, the force between the molecules will fix the position and the molecules will not move even if light is absent (Figure 1c). Thus, the orientation of azo dyes produced by the linear polarization is complete.

2.2. Polarization Absorption of Photoalignment Materials. Brilliant yellow (BY), a commercially available azo dye, has been widely applied to LC-FOEs as PA agents.[1−5] The chemical structure of BY is shown in Figure 2a. In experiment, the BY was diluted in 0.5 wt % dimethylformamide (Sigma-Aldrich, 99%, water content ⩽0.5%) and then spin-coated on a clean glass substrate at 1500 rpm for 30 s. We measured the polarized absorption spectra at room temperature under different conditions: exposure energy (linearly polarized UV light ($\lambda \approx 365$ nm) at 0.4, 1.0, and 2.5 J/cm^2), with or without soft baking (90 °C for 20 min); the measured beam is parallel (A_{para}) or perpendicular (A_{perp}) to the molecular orientation direction.

Figure 2b−d depicts the experimental results. As expected, higher exposure energy gives a larger dichroic ratio (DR = A_{para}/A_{perp}). Interestingly, we find that the DR of the nonbaking sample is higher than that of the baked one, as Figure 2b shows. Figure 2c,d shows the detailed absorption spectra with and without baking at 2.5 J/cm^2 exposure. Before UV exposure, the absorption of BY is polarization-independent (black lines). After exposure to a linearly polarized light, the redirected azo dye molecules have different absorption

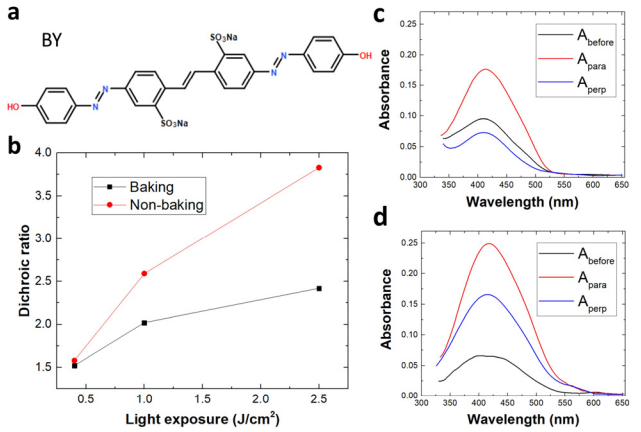

Figure 2. (a) Chemical structure of brilliant yellow. (b) Measured DR and absorption spectra at 2.5 J/cm^2 (c) with and (d) without soft baking.

responses to the measurement beam whose polarization direction is perpendicular or parallel to the absorption oscillator. When the polarization direction of the measurement beam is perpendicular to the redirected absorption oscillator, the absorption decreases (blue lines). On the contrary, when they are parallel, the absorption is stronger (red lines). Because of this unique polarized absorption behavior, azo dyes have been commonly used for PA applications, especially for LC-based photonic devices.

3. APPLICATION OF PHOTOALIGNMENT FOR ULTRATHIN FLAT OPTICS

3.1. Polarization Field Generation. As mentioned above, the azo dyes respond to and record the polarized light fields. After exposure, the patterned PA layer will replicate the alignment patterns to the LC monomer lying on top. Commonly utilized approaches to generate polarization fields for LC-FOEs can be categorized into two types: interferometry and noninterferometry.

The most widely used exposure setups are two-beam interferometry[18] and Mach−Zehnder[1] interferometry, as illustrated in Figure 3a,b. The linearly polarized beam from the laser is split into two arms and then converted to circular polarization (CP). When two CP beams with opposite handedness interfere at the sample position, the electric field on the sample plane exhibits a sinusoidal linear polarization pattern, which is recorded by the PA layer. This simple setup with a large interference angle is suitable for fabricating optical elements with a small periodicity, such as gratings or lenses whose period is several hundreds of nanometers.[14] Different from the two-beam method, the Mach−Zehnder interferometry limits the interference to a small angle. This is suitable for fabricating large period optical elements, such as gratings or lenses with a period up to several tens of micrometers.[1] In addition, Sagnac interferometry (Figure 3c) with high stability[1] and standing wave interferometry (Figure 3d) with doubled efficiency[19] has also been demonstrated recently.

In the noninterferometry approach, the desired polarization fields can be generated by a spatial light modulator (SLM) or direct writing, as illustrated in Figure 3e,f, respectively. An important advantage of using SLM is its convenience to provide a one-shot arbitrary pattern without complex interference.[20] In contrast to SLM, direct writing generates a

https://dx.doi.org/10.1021/acsomega.0c05087
ACS Omega 2020, 5, 31485−31489

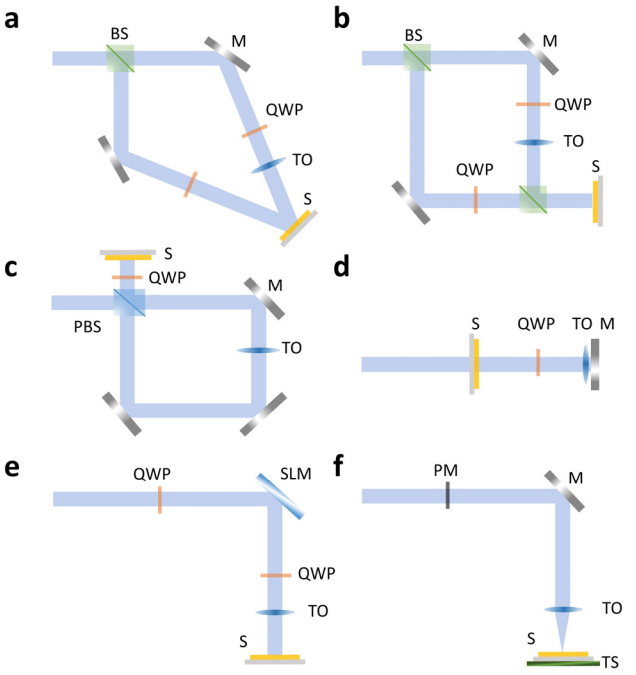

Figure 3. Experimental setups of the exposure pattern generation. Interferometry types: (a) two-beam, (b) Mach–Zehnder, (c) Sagnac, and (d) standing wave. Noninterferometry types: (e) polarization holography by a SLM and (f) polarization direct-write (BS, beam splitter; M, mirror; QWP, quarter-wave plate; TO, template optics; S, sample; PBS, polarizing beam splitter; PM, polarization modulator; TS, translation stage).

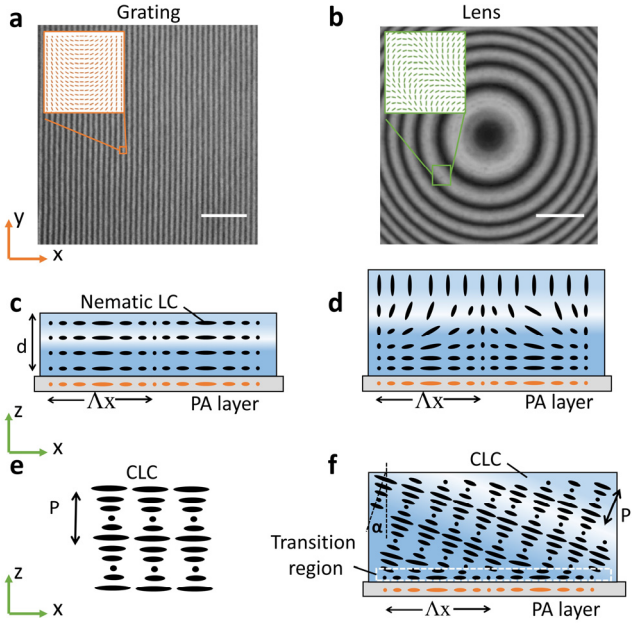

Figure 4. Polarizing optical microscope images of LC-based flat optics: (a) grating and (b) lens. The scale bar is 50 μm, and the insets are the local LC molecular directions. (c) Formation of in-plane sinusoidal structure. (d) Distortion of sinusoidal structure. (e) CLC helical structure and (f) tilted CLC structure.

designed pattern by scanning a focused laser beam to a sample placed on a translation stage.[21]

3.2. LC Orientation and Dynamics. Different exposure patterns would generate different LC-FOEs, including but not limited to gratings, lenses, lens array, vortex retarders, and other complex optics. Among them, LC-based gratings and lenses have been widely investigated and utilized in near-eye display systems. Figure 4a,b depicts the polarized optical microscopy images of the LC grating and lens, respectively. If we zoom into a small area, as the insets in Figure 4a,b show, the LC director orientation is periodically and continuously rotated according to the sinusoidal PA patterns in the x–y plane.

When a nematic LC is placed on top of the sinusoidal photoalignment pattern, the bottom LC molecules tend to follow the pattern and then transfer the pattern to the bulk along z direction. This whole process can be described by the Oseen–Frank model,[22] where the total free energy for surface and bulk interactions is minimized. When the sample thickness (d) is smaller than the pattern period, the bulk LC molecules can maintain the in-plane sinusoidal pattern, as shown in Figure 4c. As d gets larger or the grating period becomes smaller, the bulk LC will deviate from the planar alignment and start to orient toward the substrate normal,[23,24] as Figure 4d shows. This behavior can be intuitively understood by the fact that the most relaxed state for nematic LC is the uniform distribution, which corresponds to the zero free energy. The sinusoidal in-plane LC orientation is a distorted state and has a higher free energy. As the thickness increases, the confining power of the bottom pattern becomes weaker and the upper LC molecules tend to relax to the uniform state. If an electric field is applied to the bulk LC, the total free energy would include the term responding to the field–molecule interaction. The LC molecules will tend to align along or perpendicular to the electric field, depending on the dielectric anisotropy of the employed LC. As the voltage keeps increasing, the bulk LC molecules will be eventually reoriented by the electric field. As a result, the grating pattern and the associated diffraction behavior disappears. This dynamic switching behavior of diffraction has found useful applications in imaging and display devices.

Aside from nematic, we can also use cholesteric liquid crystal (CLC), which can be formulated by doping some chiral agents to a nematic host. The most relaxed state of an CLC is the helical structure depicted in Figure 4e, whose pitch P is determined by the chiral concentration and helical twisting power. If a CLC is placed on the sinusoidal pattern instead, the situation becomes more complicated. On one hand, the bottom LC in contact with the photoalignment layer still tends to follow the pattern. On the other hand, the bulk LCs tend to maintain an ideal helical structure to minimize the free energy. The only way to satisfy both conditions is to tilt the bulk helical structure to match the k-vector of the bottom pattern,[22] as shown in Figure 4f. This indicates the tilt angle α should satisfy $P = \Lambda_x \cos \alpha$, where Λ_x is the horizontal period. The tilted structure brings a transitional region where the LC molecules transit from the bottom in-plane orientation to the tilted helical structure. The thickness of the transition region is usually tens of nanometers, so the contribution of this region to the total energy is very small. Here, we make a presumption that the CLC pitch is smaller than the pattern period. Otherwise, no matter how the CLC is tilted, the matching of the bottom wave-vector cannot happen. If an electric field is applied to the tilted CLC structure, the tilt angle will begin to increase.[24] As the voltage increases, the CLC helical axis will be reoriented to be parallel to the substrate surface. This structure is known as uniform lying helix (ULH). As the voltage keeps

https://dx.doi.org/10.1021/acsomega.0c05087
ACS Omega 2020, 5, 31485–31489

increasing, the ULH will be distorted toward the field direction until the helical structure is completely unwound by the electric field.

3.3. Optical Properties. Due to different LC orientations inside the volume, LC-FOEs are usually divided into transmissive type (patterned nematic LC) and reflective type (patterned CLC). The operation principle of transmissive LC flat optics can be simply explained by Jones calculus:

$$\begin{cases} J_{\pm} = \frac{1}{\sqrt{2}}\begin{bmatrix} 1 \\ \pm j \end{bmatrix} \\ J'_{\pm} = R(-\psi)W(\pi)R(\psi)J_{\pm} = -je^{\pm 2j\psi}J_{\mp} \end{cases} \quad (1)$$

where J is the Jones vectors of circularly polarized light, R is the rotation matrix, W is the half-wave retardation Jones matrix, and ψ is the local LC director orientation angle. The subscripted $\pm$ signs indicate the left- and right-handed circular polarization (LCP and RCP) states. From eq 1, the accumulated phase is opposite for LCP and RCP lights. As depicted in Figure 5a,b, a transmissive LC grating will deflect RCP and LCP to opposite directions, and a lens will focus RCP but defocus LCP light.[25]

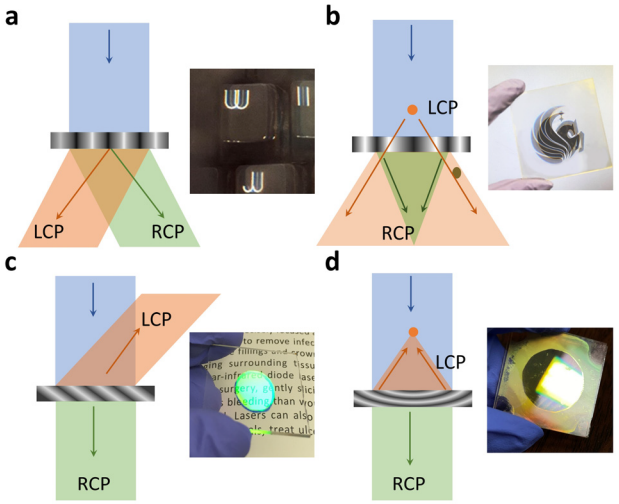

Figure 5. Illustration and photos of LC optics. Transmissive type: (a) a grating diffracts RCP light to +1 order and LCP light to −1 order; (b) a lens diverges the input LCP light but converges the RCP light. Reflective type: (c) a grating diffracts LCP light and transmits RCP light; (d) a lens reflects and converges the incident LCP light but transmits the RCP. Photograph courtesy of Kun Yin. Copyright 2020. The image is free domain.

The reflective LC-FOEs work under Bragg condition. It enables tunable spectral bandwidth and manifests more sensitive spectral and angular responses than the transmissive type. A typical CLC device can be realized by self-organized molecules to form a helical structure. If the incident circularly polarized light (e.g., LCP) has the same handedness as the helical twist, then it will experience Bragg reflection at normal incidence over the spectral range $2n_oP < \lambda < 2n_eP$, where n_o and n_e are the ordinary and extraordinary refractive indices. Meanwhile, the RCP will pass through the CLC layer. Therefore, unlike transmissive LC flat optics, ordinary reflective LC flat optics only works for one polarization handedness, and the other will be transmitted without changing its polarization state (Figure 5c,d).

It is worth mentioning that both transmissive and reflective LC-FOEs can achieve nearly 100% diffraction efficiency. The thickness of each element can be controlled between several hundreds of nanometers and several microns, depending on the working type. By applying more complex structures, such as multilayers and gradient pitch, we can obtain LC flat optics with a wide viewing angle and broadband while maintaining a high efficiency and ultrathin form factor.

4. CONCLUSIONS

In this mini-review, we briefly summarize the mechanism of PA and optical properties of LC-FOEs. To understand the PA mechanism of azo dyes, we use the diffusion model to explain the photoinduced process and take brilliant yellow as an example to investigate the dichroic ratio under different conditions. Based on the polarized response of azo dyes, it is feasible to record various patterns through appropriate exposure methods. The LC molecules follow the recorded pattern and precisely organize the vertical structures for building planar optical elements. Due to the unique molecular dynamics and polarization selectivity, LC-FOEs with ultrathin form factor have found widespread applications in novel optical systems, particularly virtual/augmented/mixed reality displays and head-up displays.

AUTHOR INFORMATION

Corresponding Author

Shin-Tson Wu − *College of Optics and Photonics, University of Central Florida, Orlando, Florida 32816, United States;* orcid.org/0000-0002-0943-0440; Email: swu@creol.ucf.edu

Authors

Kun Yin − *College of Optics and Photonics, University of Central Florida, Orlando, Florida 32816, United States*

Jianghao Xiong − *College of Optics and Photonics, University of Central Florida, Orlando, Florida 32816, United States*

Ziqian He − *College of Optics and Photonics, University of Central Florida, Orlando, Florida 32816, United States*

Complete contact information is available at: https://pubs.acs.org/10.1021/acsomega.0c05087

Notes

The authors declare no competing financial interest.

Biographies

Kun Yin received her B.S. degree in Optoelectronics from Tianjin University in 2016 and is currently working toward a Ph.D. from the College of Optics and Photonics, University of Central Florida, Orlando. Her current research interests include novel optical components based on liquid-crystal materials and optical system design for augmented reality and virtual reality displays.

Jianghao Xiong received his B.S. degree in Physics from the University of Science and Technology of China in 2017 and is currently working toward a Ph.D. from the College of Optics and Photonics, University of Central Florida, Orlando. His current research interests include near-eye displays and novel liquid-crystal display devices.

Ziqian He received his B.S. degree in Material Physics from Nanjing University in 2016 and is currently working toward a Ph.D. from the College of Optics and Photonics, University of Central Florida. His current research interests include novel liquid-crystal devices, nanocrystals, and color science.

https://dx.doi.org/10.1021/acsomega.0c05087
ACS Omega 2020, 5, 31485−31489

Shin-Tson Wu is a Pegasus professor at the College of Optics and Photonics, University of Central Florida. He is among the first six inductees of the Florida Inventors Hall of Fame (2014) and a Charter Fellow of the National Academy of Inventors (2012). He is a fellow of the IEEE, OSA, SID, and SPIE. He is the recipient of OSA Esther Hoffman Beller Medal (2014), SID Slottow-Owaki Prize (2011), OSA Joseph Fraunhofer Award (2010), SPIE G. G. Stokes Award (2008), and SID Jan Rajchman Prize (2008).

■ ACKNOWLEDGMENTS

The authors are indebted to GoerTek Electronics for the financial support.

■ REFERENCES

(1) Zhan, T.; Lee, Y. H.; Tan, G.; Xiong, J.; Yin, K.; Gou, F.; Zou, J.; Zhang, N.; Zhao, D.; Yang, J.; Liu, S.; Wu, S. T. Pancharatnam–Berry optical elements for head-up and near-eye displays. *J. Opt. Soc. Am. B* **2019**, *36*, D52–D65.

(2) Yin, K.; Zhan, T.; Xiong, J.; He, Z.; Wu, S. T. Polarization Volume Gratings for Near-eye Displays and Novel Photonic Devices. *Crystals* **2020**, *10*, 561.

(3) Yin, K.; Lin, H. Y.; Wu, S. T. Chirped polarization volume grating for wide FOV and high efficiency waveguide-based AR displays. *J. Soc. Inf. Disp.* **2020**, *28*, 368–374.

(4) Zhan, T.; Yin, K.; Xiong, J.; He, Z.; Wu, S. T. Augmented reality and virtual reality: perspectives and challenges. *iScience* **2020**, *23*, 101397.

(5) Zou, J.; Hsiang, E. L.; Zhan, T.; Yin, K.; He, Z.; Wu, S. T. High Dynamic Range Head-up Display. *Opt. Express* **2020**, *28*, 24298–24307.

(6) Schadt, M.; Seiberle, H.; Schuster, A. Optical patterning of multi-domain liquid-crystal displays with wide viewing angles. *Nature* **1996**, *381*, 212–215.

(7) He, Z.; Lee, Y. H.; Chen, R.; Chanda, D.; Wu, S. T. Switchable Pancharatnam-Berry microlens array with nano-imprinted liquid crystal alignment. *Opt. Lett.* **2018**, *43*, 5062–5065.

(8) Chigrinov, V. G.; Kozenkov, V. M.; Kwok, H. S. *Photoalignment of Liquid Crystalline Materials: Physics and Applications.*; John Wiley & Sons, 2008.

(9) Kvasnikov, E. D.; Kozenkov, V. M.; Barachevsky, V. A. Birefringence in Polyvinylcinnamate Films Induced by Polarized Light. *Doklady AN SSSR* **1977**, *237*, 633–636.

(10) Ichimura, K.; Suzuki, Y.; Seki, T.; Hosoki, A.; Aoki, K. Reversible change in alignment mode of nematic liquid crystals regulated photochemically by command surfaces modified with an azobenzene monolayer. *Langmuir* **1988**, *4*, 1214–1216.

(11) Gibbons, W. M.; Shannon, P. J.; Sun, S. T.; Swetlin, B. J. Surface-mediated alignment of nematic liquid crystals with polarized laser light. *Nature* **1991**, *351*, 49.

(12) Schadt, M.; Schmitt, K.; Kozinkov, V.; Chigrinov, V. Surface-induced parallel alignment of liquid crystals by linearly polymerized photopolymers. *Jpn. J. Appl. Phys.* **1992**, *31*, 2155.

(13) Yin, K.; Lee, Y. H.; He, Z.; Wu, S. T. Stretchable, flexible, rollable, and adherable polarization volume grating film. *Opt. Express* **2019**, *27*, 5814–5823.

(14) Yin, K.; He, Z.; Wu, S. T. Reflective polarization volume lens with small f-number and large diffraction angle. *Adv. Opt. Mater.* **2020**, *8*, 2000170.

(15) Pedersen, T. G.; Ramanujam, P. S.; Johansen, P. M.; Hvilsted, S. Quantum theory and experimental studies of absorption spectra and photoisomerization of azobenzene polymers. *J. Opt. Soc. Am. B* **1998**, *15*, 2721.

(16) Akiyama, H.; Kawara, T.; Takada, H.; Takatsu, H.; Chigrinov, V.; Prudnikova, E.; Kozenkov, V.; Kwok, H. Synthesis and properties of azo dye aligning layers for liquid crystal cells. *Liq. Cryst.* **2002**, *29*, 1321.

(17) Nishikawa, M.; Taheri, B.; West, J. L. Mechanism of unidirectional liquid-crystal alignment on polyimides with linearly polarized ultraviolet light exposure. *Appl. Phys. Lett.* **1998**, *72*, 2403–2405.

(18) Gao, K.; McGinty, C.; Payson, H.; Berry, S.; Vornehm, J.; Finnemeyer, V.; Roberts, B.; Bos, P. High-efficiency large-angle Pancharatnam phase deflector based on dual-twist design. *Opt. Express* **2017**, *25*, 6283–6293.

(19) He, Z.; Yin, K.; Wu, S. T. Standing wave polarization holography for realizing liquid crystal Pancharatnum-Berry phase lenses. *Opt. Express* **2020**, *28*, 21729–21736.

(20) De Sio, L.; Roberts, D. E.; Liao, Z.; Nersisyan, S.; Uskova, O.; Wickboldt, L.; Tabiryan, N.; Steeves, D. M.; Kimball, B. R. Digital polarization holography advancing geometrical phase optics. *Opt. Express* **2016**, *24*, 18297–18306.

(21) Miskiewicz, M. N.; Escuti, M. J. Direct-writing of complex liquid crystal patterns. *Opt. Express* **2014**, *22*, 12691–12706.

(22) Xiong, J.; Chen, R.; Wu, S. T. Device simulation of liquid crystal polarization gratings. *Opt. Express* **2019**, *27*, 18102–18112.

(23) Komanduri, R. K.; Escuti, M. J. Elastic continuum analysis of the liquid crystal polarization grating. *Phys. Rev. E* **2007**, *76*, 021701.

(24) Sarkissian, H.; Park, B.; Tabirian, N.; Zeldovich, B. Periodically Aligned Liquid Crystal: Potential Application for Projection Displays. *Mol. Cryst. Liq. Cryst.* **2006**, *451*, 1–19.

(25) Li, Y.; Liu, Y.; Li, S.; Zhou, P.; Zhan, T.; Chen, Q.; Su, Y.; Wu, S.-T. Single-exposure fabrication of tunable Pancharatnam-Berry devices using a dye-doped liquid crystal. *Opt. Express* **2019**, *27*, 9054–9060.

https://dx.doi.org/10.1021/acsomega.0c05087
ACS Omega 2020, 5, 31485–31489